



<https://technobius.kz/>

e-ISSN  
3007-0147

# Technobius Physics

*A peer-reviewed open-access journal*

*Technobius, LLP*

*Volume 1, No. 3, 2023*



# Technobius Physics

Volume 1, No. 3, 2023



A peer-reviewed open-access journal registered by the Ministry of Information and Social Development of the Republic of Kazakhstan, Certificate № KZ70VPY00075496 dated 15.08.2023




**ISSN (Online):** 3007-0147

**Thematic Directions:** General Physics, Condensed Matter Physics




**Publisher:** Technobius, LLP

**Address:** 2 Turkestan street, office 116, 010000, Astana, Republic of Kazakhstan

















**Editor-in-Chief:**

   *Aida Nazarova*, PhD, Laboratory Assistant, Department of Physics, Nazarbayev University, Astana, Kazakhstan

**Technical Editor:**

   *Saeed Nasiri*, Dr, Professor, Department of Physics, Nazarbayev University, Astana, Kazakhstan

**Editors:**

-   *Sang Ma Lee*, Dr., Professor, Engineering Research Center for Net Shape and Die Manufacturing, Pusan National University, Busan, South Korea
-   *Suk Bong Kang*, Dr., Professor, Korea Institute of Materials Science, Changwon, South Korea
-   *Marshall Onellion*, Dr., Professor, Department of Physics, University of Wisconsin-Madison, Madison, United States
-    *Bill Wheatle*, Dr, Assistant Professor, McKetta Department of Chemical Engineering, The University of Texas at Austin, Austin, United States
-   *Hyun-ho Kim*, Dr, Assistant Professor, School of Mechanical Engineering, Pusan National University, Busan, South Korea
-   *Yong-phil Jeon*, Dr., Precision Manufacturing System Division, Pusan National University, Busan, South Korea
-    *Marius Schwarz*, Dr., Assistant Professor, Department of Civil Engineering, University North, Varaždin, Croatia

**Copyright:** © Technobius, LLP

**Contacts:** Website: <https://technobius.kz/>  
E-mail: [technobiusphysics@gmail.com](mailto:technobiusphysics@gmail.com)

**CONTENTS**

<b>Title and Authors</b>	<b>Category</b>	<b>No.</b>
Stability of dielectric properties of aluminum under gamma-quantum irradiation <i>Adilzhan Omarov, Aigul Zhantasova, Almas Siddiqui</i>	<i>Condensed Matter Physics</i>	0001
The function of the time constant in RC series circuit signal filtering <i>Nurbek Isayev, Serik Kurmanov</i>	<i>General Physics</i>	0002
Experimental investigation of electron-mercury atom collisions: insights into atomic interaction dynamics <i>Daniyar Yesengaliev, Adolf Kim, Alisher Yeskenbayev, Kairbek Zhetpisbayev</i>	<i>Condensed Matter Physics</i>	0003



## Stability of dielectric properties of aluminum under gamma-quantum irradiation

Adilzhan Omarov<sup>1,\*</sup>, Aigul Zhantasova<sup>1</sup>, Almas Siddiqui<sup>2</sup>

<sup>1</sup>Faculty of Computer Science, Toraighyrov Pavlodar University, 64 Lomov st., Pavlodar, Kazakhstan

<sup>2</sup>Division of Physical and Mathematical Sciences, Indian Institute of Science Bangalore, 54 Raman Rd., Bengaluru, India

\*Correspondence: [omarov.adilzhan@list.ru](mailto:omarov.adilzhan@list.ru)

**Abstract.** In this work was to reveal the effects of gamma-quantum irradiation on the microstructure and electrophysical characteristics of aluminum. The effects of gamma irradiation with a radionuclide source of cesium-137 isotope on the properties of aluminum were studied. The maximum absorbed doses were approximately  $10^8$  rads. Aluminum plates with a thickness of 6 mm and an area of  $5 \text{ cm}^2$  were utilized during the experiments. The main challenge in obtaining reliable, Adequate automated adaptation of the gamma spectrometer under conditions of change in a certain range of characteristics of the water environment (such as, for example, temperature and pressure) is the task of obtaining reliable, high-quality and reliable measurements. The paper presents the results of testing and adjustment of the complex of autonomous automated calibration of  $^{137}\text{Cs}$  gamma-spectrometer. The processes occurring during gamma-quantum irradiation of aluminum and their influence on dielectric properties of the material were studied. The results obtained indicate that when aluminum is irradiated with a dose of  $10^8$  rad, only a slight change in its dielectric permittivity is observed.

**Keywords:** gamma ray, irradiation,  $^{137}\text{Cs}$  isotope, semiconductors, aluminum.

### 1. Introduction

It is known that irradiation of metals, semiconductor crystals and alloys with gamma quanta can lead to disruption of their structure by introducing radiation defects [1-3]. These defects can include point defects such as vacancies and interstitial atoms as well as linear defects such as dislocations. Radiation defects can affect the mechanical, electrical, and magnetic properties of materials, making gamma ray irradiation an important factor in studying the behavior of materials under radiation exposure.

However, in the study [4-5] it was found that the irradiation of metals, semiconductors and alloys by gamma-quanta with an exposure dose of more than  $10^5$  J/kg does not lead to the accumulation of defects, but, on the contrary, promotes their elimination and leads to the transition of the material to a more stable state compared to its initial state. An interesting phenomenon is that such effects of ionizing radiation cause rearrangement of the metal structure and consequently lead to changes in its electrophysical properties.

In the modern electrical industry, considerable importance is attached to the use of aluminum and its oxides because of their semiconducting properties [6-7]. These materials offer a number of advantages such as high thermal conductivity, strength and low density, making them an ideal choice for many applications in electronics and electrical engineering. Their use enables the creation of components with high efficiency and reliability, which is important for modern technology and industrial processes.

Other scientists have studied the effect of ionizing radiation on the stability of semiconductor devices [8-9]. Moreover, gamma radiation has a particularly negative impact, as it has a high

penetrating ability and is characterized by the lack of effective protection methods. This property of gamma radiation makes it especially dangerous for semiconductor devices, as it is able to penetrate through ordinary materials and cause significant changes in their structure and functionality. As a result, the development of methods of protection against gamma radiation and the study of its effects on semiconductor devices are important areas of research in the field of electronics and electrical engineering [10]. Therefore, the main aspect of our study is to investigate the effect of gamma rays on the characteristics of aluminum.

The primary challenge in achieving accurate and high-quality measurements lies in implementing an effective automated adaptation mechanism for the gamma-spectrometer, particularly when faced with variations in key environmental parameters within the water medium, such as temperature and pressure. This paper outlines the outcomes of testing and fine-tuning procedures conducted on the autonomous automated calibration system for Cs137 gamma-spectrometers.

## 2. Methods

In this work, optical and mechanical experimental methods were used to study radiation damage in the structure of an irradiated aluminum plate sample, both in the volume and in the surface layer with gamma radiation sources of radioactive isotopes Cs<sup>137</sup> of 662 keV. The number of radiation sources, their location and the configuration of the chamber guaranteed a uniform gamma ray flux. The irradiation was performed in a closed chamber containing oxygen at normal room temperature. The irradiation rate was constant at 65 rad/s, and the maximum absorbed doses were  $\sim 10^8$  rads. Aluminum plates were used with a thickness of 6 mm, area 5 cm<sup>2</sup>.

A gamma radiation source of the Cs<sup>137</sup> crystals were used as ionizing radiation, the flashes of which were recorded using light-sensitive devices as a photomultiplier tube (PMT) based on NaI (TI) crystal.

The NaI (TI) scintillation detector coupled with a PMT operates as a highly efficient system for detecting and measuring gamma rays and other forms of ionizing radiation. The core component, the NaI (TI) crystal, is a thallium-doped sodium iodide scintillator, which plays a crucial role in the detection process [11].

Figure 1 presents a block diagram illustrating the configuration of the spectrometer system.

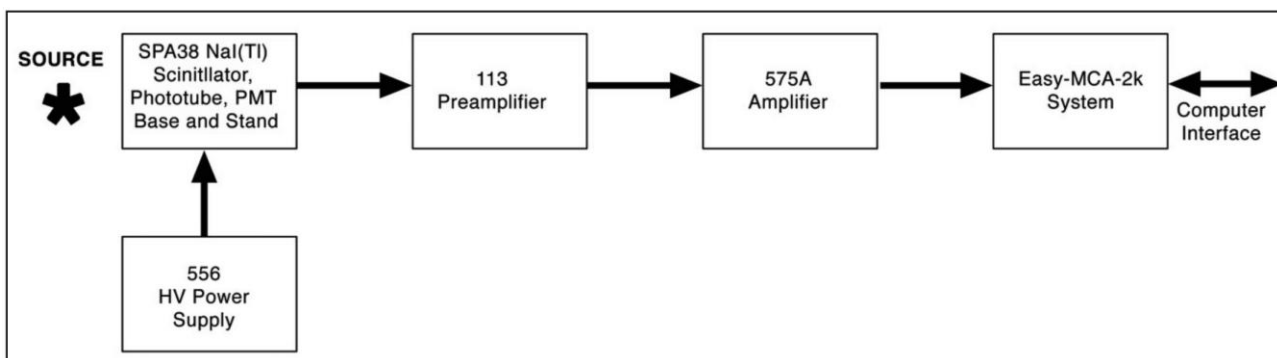


Figure 1 – Block diagram showcasing the electronics setup for a gamma-ray spectroscopy system employing a NaI (TI) detector [12]

Initially, the preamplifier gathers the charge accumulated on the anode via a capacitor, converting this charge into a voltage pulse. This pulse is then relayed to the subsequent amplifier for further processing. The magnitude of the voltage pulse at both the output of the preamplifier and the output of the linear amplifier is directly proportional to the energy imparted to the scintillator by the gamma ray being detected [12].

The Universal Computer Spectrometer (UCS) system is specifically engineered to interface seamlessly with personal computers via a USB connection. To ensure both stable performance and

minimal noise interference, the device utilizes an alternating current (AC) power source, accommodating a wide voltage range from 100 to 250 V AC through an automatically adjusting power supply. The device incorporates a microprocessor that functions as the central processing unit and data storage medium, facilitating direct communication with the PC through the USB interface.

As a calibration sample was used Cs<sup>137</sup> isotopes of round shape, 2.5 cm in diameter, which were placed on a tray located on the secondary rack. The parameters of gamma irradiation were set as follows: voltage 450 V, number of channels – 1024, fine grain – 1.0, course gain – 16, lower discriminator – 0, upper discriminator - 1024. After an interval of 500 seconds, spectral data were acquired. Reference values corresponding to characteristic isotope peaks were used to ensure the accuracy of the energy calibration. Control of calibration accuracy consists in calculation of backscattering peaks and Compton edge.

After this calibration, the accuracy of registration is checked by calculation of backscatter peaks and Compton edge. At this stage, the Cs<sup>137</sup> sample is moved to the third rack of the experimental setup and then an aluminum plate is installed.

Optical absorption spectra were measured on a Phywe spectrometer corrected for the thickness of each sample. The mass absorption coefficient of the aluminum plate sample was determined, which is found using Lambert's Law about the decrease of intensity of radiation [13]:

$$I = I_0 e^{-\mu x} \quad (1)$$

Where:  $I$  – intensity after the absorber;  $I_0$  – intensity before the absorber;  $\mu$  – total-mass absorption coefficient,  $cm^2/g$ ;  $x$  - density thickness  $g/cm^2$ .

To determine the absorption coefficient, the natural logarithm of the ratio  $\ln \frac{I}{I_0} = -\mu x$  was plotted and fitted to a linear regression line, where  $\frac{N}{N_0} = \frac{I}{I_0}$  represents the net number of counts obtained in each measurement with the aluminum plate placed between the source and detector, and  $N_0$  denotes the number of counts obtained without attenuation. The intensity  $I$  is proportional to the number of samples, so  $\frac{N}{N_0}$  corresponds to the ratio of intensities  $\frac{I}{I_0}$ .

To quantify the number of samples, a region of interest (ROI) around the 662 keV peak is defined. By selecting this region of interest in the program spectrum, the number of clean counts in this region as well as the full width half-maximum (FWHM) of the peak can be obtained. Then, by measuring the decrease in the number of clean counts in the 662 keV peak for each additional aluminum plate introduced between the source and detector, the absorption coefficient is calculated.

For an extended view, we considered the effect of gamma radiations on the dielectric properties of aluminum.

### 3. Results and Discussion

Due to their high penetrating ability, gamma quanta can affect the electrophysical characteristics of metals, semiconductors and metals [14-16].

Figure 2 depicts the dual peaks resulting from a Cs<sup>137</sup> radioisotope. The energy spectrum of cesium-137 was calibrated at 450 V and gain 16 sec. The scan area covered energies from 590 keV to 706 keV. The clean counts are displayed in the lower right corner of the software interface, thus no aluminum plates were installed between the source and detector. The decay process primarily involves a beta emission, with over 93% of occurrences, leading to the 661.6 keV excited state of Cs<sup>137</sup>.

Subsequently, decay to the ground state follows through a 661.6 keV gamma-ray emission. Additionally, there is consistently a noticeable peak of X-ray radiation at 32 keV [16-18], which serves as a calibration reference. Therefore, the main energy channel in cesium is at an energy of 662 keV, and Compton scattering is observed at an energy of 30 keV.

Two characteristic peaks are observed on the energy spectrum: the Compton edge peak and the backscattering peak, labeled with energies of 208.72 keV and 463 keV, respectively.

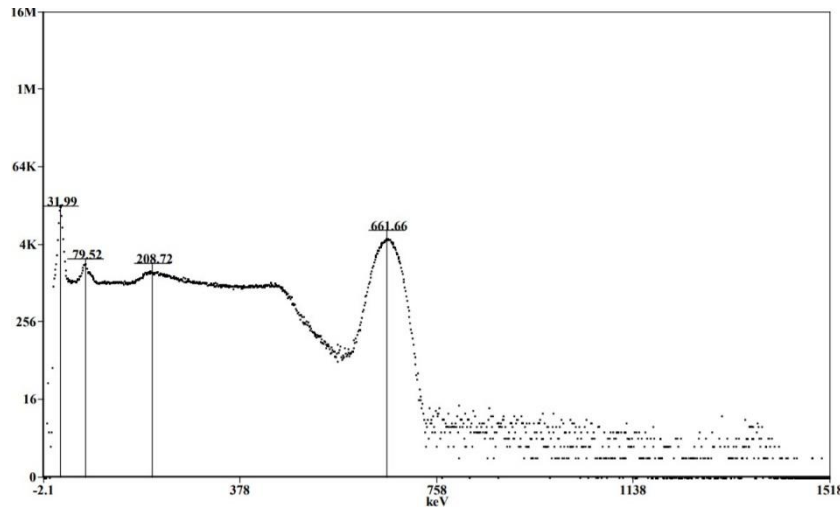


Figure 2 – Calibrated energy spectrum of Cs<sup>137</sup> at 450 V

The first of them is caused by Compton scattering of gamma-quanta on the detector electrons, and its energy is calculated according to the Compton equation at  $\Theta = 0$  using the known value of the electron rest mass  $mc^2 = 511$  keV. Accordingly, the energy of the Compton edge peak is 208.72 keV. The backscattering peak manifests itself as a result of backscattering of gamma quanta on the source electrons. Its energy corresponds to the energy of gamma quanta scattered by 180 degrees. Thus, the energy of the backscattering peak is 463 keV.

For a more accurate calculation of the photon energy after scattering of the irradiated sample of cesium isotope, we used the following formula:

$$E' = \frac{E}{1 + \frac{E}{mc^2} (1 - \cos \theta)} \quad (2)$$

Where:  $E'$  – the energy of the scattered photon, keV;  $E$  – peak energy, keV;  $m$  – the mass of the electron, kg;  $c$  – the speed of light, m/s;  $\theta$  – the angle of scattering of the gamma-ray, deg.

Figure 3 shows the gamma ray spectra of aluminum plate, which was placed between the radiation source and the detector during the measurements.

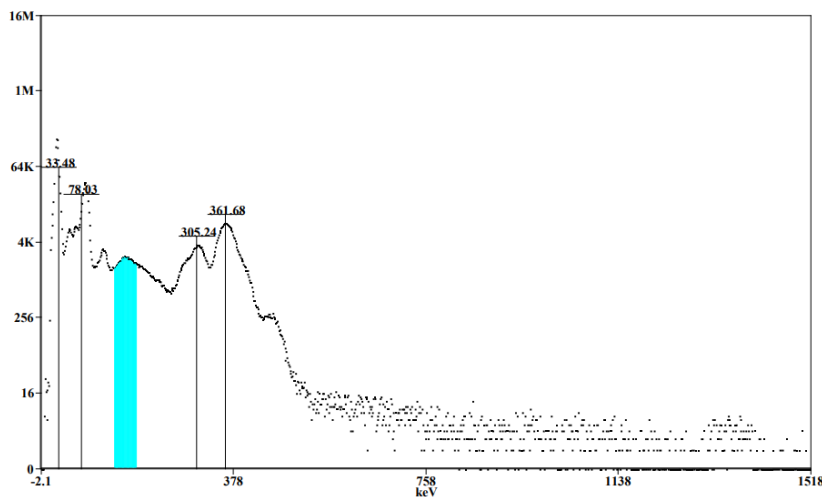


Figure 3 – A calibrated energy spectrum of <sup>137</sup>Cs acquired at a voltage of 450V and with a coarse gain setting of 16

A ROI has been defined spanning from 590 keV to 706 keV. The net counts corresponding to this ROI are displayed in the bottom right corner of the software interface. An aluminum plate was positioned between the radiation source and the detector during the measurements.

Given the premise that the energy of the scattered photon equals the sum of the energies of the scattered electron and the incident wave, we can derive the energy of the scattered electron as



follows:  $E'_e = E' = E$ , where,  $E'_e$  – the energy of the scattered electron, keV;  $E'$  – the energy of the scattered photon, keV;  $E$  – peak energy, keV.

The calculated value of the backscattering peak energy for  $^{137}\text{Cs}$  is 184.32 keV and the maximum Compton edge energy is 477.34 keV. This close agreement with theoretical expectations indicates a well-calibrated system, as it reflects the expected energy level for backscattered photons in this experimental setup [17-19].

According to the data obtained in Table 1, the number of gamma photons that deviate from the photopeak due to photoelectric or Compton interactions occurring in the aluminum absorber placed between the radiation source and the detector was detected.

Table 1 – The mass absorption coefficient of the Aluminium for E=662 keV

The theoretical mass absorption coefficient, $\text{cm}^2/\text{g}$	Experimental obtained mass absorption coefficient, $\text{cm}^2/\text{g}$
0.078	$0.063 \pm 0.007$

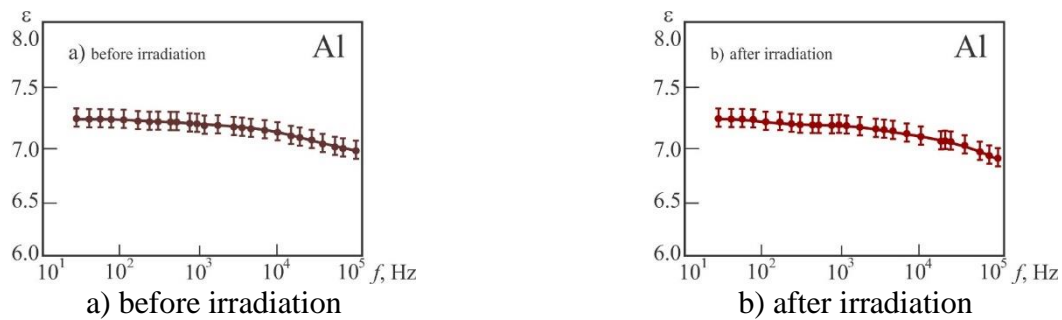


Figure 4 – The dependence of frequency on dielectric permittivity

Figure above shows the dependence of frequency on dielectric permittivity before (Figure 4a) and after (Figure 4b) irradiation. In the observed frequency range, an increase in frequency was accompanied by a slight decrease in the value of  $\epsilon$ . It was found that after irradiation of aluminum samples with  $^{137}\text{Cs}$  radionuclides to a dose of  $10^8$  rad, the dielectric constant remained almost unchanged over the entire frequency range, as shown in Figure 4b.

Due to the fact that aluminum is characterized by a forbidden zone width  $E_g$  from 5.1 to 8.8 eV, under normal conditions the concentration of electrons in the conduction band remains low, which entails negligible conductivity of this material.

#### 4. Conclusions

In this work, the effect of gamma radiation  $^{137}\text{Cs}$  isotope source irradiation on the properties of aluminum was presented, detailed calibration of the spectrophotometer was performed by decomposition of energy spectra, determination of the mass absorption coefficient of aluminum, and the dependence of the dielectric constant of aluminum on gamma radiation was shown.

As a result of the study, it was found that irradiation of aluminum samples with  $^{137}\text{Cs}$  radionuclides up to a dose of  $10^8$  rad has no significant effect on the dielectric constant of this material in a wide frequency range. The observed insignificant change in the electrical properties of aluminum after irradiation can be explained by its peculiarities, such as the width of the forbidden zone. Thus, the results of the study confirm the stability of dielectric properties of aluminum under irradiation with  $^{137}\text{Cs}$  radionuclides up to the considered irradiation dose.

#### References

1. Defects and radiation damage in metals / M.W. Thompson. — Cambridge, UK: University press, 1969. — 394 p.
2. Point Defects in Solids / A. Holland. — New York, USA: Springer, 1972. — 556 p.
3. Dynamics of annihilation of defects in semiconductor crystals under the action of small radiation doses / P.A. Cherdantsev, I.P. Chernov, Yu.A. Timoshnikov, V.A. Korotchenko, A.P. Mamontov // Soviet physics. Semiconductors. — 1984. — Vol. 18, No. 11. — P. 1283–1285.



4. Chain annihilation of defects in semiconductor crystals / P.A. Cherdantsev, I.P. Chernov, A.P. Mamontov // Soviet physics. Semiconductors. — 1982. — Vol. 16, No. 3. — P. 305–308.
5. Mechanism of radiation ordering of semiconductor crystals by means of low doses of irradiation / P.A. Cherdantsev, I.P. Chernov, A.P. Mamontov // Radiation effects. — 1982. — Vol. 60, No. 1–4. — P. 67–71. <https://doi.org/10.1080/00337578208242777>
6. High- $\kappa$  gate dielectrics: Current status and materials properties considerations / G.D. Wilk, R.M. Wallace, J.M. Anthony // J. Appl. Phys. — 2001. — Vol. 89. — P. 5243–5275. <https://doi.org/10.1063/1.1361065>
7. Atomic layer deposition of titanium dioxide films using a metal organic precursor (C<sub>12</sub>H<sub>23</sub>N<sub>3</sub>Ti) and H<sub>2</sub>O (DI water) / B. Kim, N. Lee, S. Park, T. Park, J. Song, S. Han, H. Park, D. Lee, H. Kim, H. Jeon // Journal of Alloys and Compounds. — 2021. — Vol. 857. — P. 157931. <https://doi.org/10.1016/j.jallcom.2020.157931>
8. Particle interaction and displacement damage in silicon devices operated in radiation environments / C. Leroy, P.G. Rancoita // Reports on Progress in Physics. — 2007. — Vol. 70. No. 4. — P. 493. <https://doi.org/10.1088/00344885/70/4/R01>
9. Effects of  $\gamma$ -radiation on dielectric properties of LDPE–Al<sub>2</sub>O<sub>3</sub> nanocomposites / F. Ciuprina, T. Zaharescu, I. Pleșa // Radiation Physics and Chemistry. — 2013. — Vol. 84. — P. 145–150. <https://doi.org/10.1016/j.radphyschem.2012.06.028>
10. Total ionizing dose effects in MOS oxides and devices / T.R. Oldham, F.B. McLean // IEEE Transactions on Nuclear Science. — 2003. — Vol. 50. No. 3. — P. 483–499. <https://doi.org/10.1109/TNS.2003.812927>
11. The photo-multiplier radiation detector / Marshall, Fitz-Hugh, J. W. Coltman, A. I. Bennett // Review of Scientific Instruments. — 1948. — Vol. 19. No. 11. — P. 744–770. <http://doi.org/10.1063/1.1741156>
12. Gamma-Ray Spectroscopy Using NaI(Tl) [Electronic resource]. — [2017]. — Mode of access: <https://www.ortec-online.com/-/media/ametektortec/third%20edition%20experiments/3-gamma-ray-spectroscopy-using-nai-tl.pdf> (accessed date: 18.07.2023).
13. The distribution in direction of photoelectrons from alkali metal surfaces / I.E. Herbert, A.R. Olpin, A.L. Johnsrud // Physical Review. — 1928. — Vol. 32. No. 1. — P. 57–80. <https://doi.org/10.1103/PhysRev.32.57>
14. The dielectric properties and radiation resistance of aluminum oxide layers obtained by atomic layer deposition / D. Dolzhenko, V. Kapralova, N. Sudar // Proceedings of the 2018 IEEE International Conference on Electrical Engineering and Photonics. — 2018. — P. 8564381. <https://doi.org/10.1109/EEExPolytech.2018.8564381>
15. Neutron and Gamma Irradiation Effects on Power Semiconductor Switches / G. E. Schwarze, A. J. Frasca // Nasa Technical Memorandum. — 1990. — Vol. 1. — P. 103200.
16. Metal and Alloy Bonding - An Experimental Analysis / M. Prema Rani, R. Saravanan. — New York, USA: Springer, 2012. — 151 p.
17. Health Physics and Radiological Health, 4th Edition. / D. Pfeiffer // Medical Physics. — 2013. — Vol. 40, No. 11. — P. 117301. <https://doi.org/10.1118/1.4826186>
18. NNDC | National Nuclear Data Center [Electronic resource]. — [2023]. — Mode of access: <https://www.nndc.bnl.gov/> (accessed date: 18.07.2023).
19. Table of Radioactive Isotopes Database [Electronic resource]. — [2023]. — Mode of access: <https://application.wiley-vch.de/books/info/0-471-35633-6/toi99/www/decay/tori.htm> (accessed date: 18.07.2023).

### Information about authors:

*Adilzhan Omarov* – Master Student, Faculty of Computer Science, Toraighyrov Pavlodar University, 64 Lomov st., Pavlodar, Kazakhstan, [omarov.adilzhan@list.ru](mailto:omarov.adilzhan@list.ru)

*Aigul Zhantasova* – Master Student, Faculty of Computer Science, Toraighyrov Pavlodar University, 64 Lomov st., Pavlodar, Kazakhstan, [zhantasova.aigul@mail.ru](mailto:zhantasova.aigul@mail.ru)

*Almas Siddiqui* – PhD Student, Division of Physical and Mathematical Sciences, Indian Institute of Science Bangalore, 54 Raman Rd., Bengaluru, India, [almsiddiqui@gmail.com](mailto:almsiddiqui@gmail.com)

### Author Contributions:

*Adilzhan Omarov* – concept, methodology, funding acquisition, testing.

*Aigul Zhantasova* – interpretation, editing, modeling, resources.

*Almas Siddiqui* – visualization, analysis, data collection, drafting.

*Received: 16.08.2023*

*Revised: 17.08.2023*

*Accepted: 24.08.2023*

*Published: 25.08.2023*



## The function of the time constant in RC series circuit signal filtering

 Nurbek Isayev\*,  Serik Kurmanov

Faculty of Digital Technologies and Arts, Turan University, 16a Satpaeva st., Almaty, Kazakhstan

\*Correspondence: [isayev\\_nurbek@mail.ru](mailto:isayev_nurbek@mail.ru)

**Abstract.** Battery storage systems are essential components in the realm of renewable energy systems and electric vehicles, providing critical support in managing power supply and demand. However, a prevalent issue within these systems is charge imbalance among individual battery cells, which can lead to suboptimal power efficiency, reduced reliability, and potential safety hazards. Addressing this challenge, researchers have focused on developing battery equalization techniques to ensure uniform charge distribution. Among the various strategies, switched-capacitor-based battery equalizers have emerged as a promising solution due to their cost-effectiveness, compact design, and controllability. This paper delves into the analysis of several switched-capacitor-based battery equalizers, including conventional, two-level, modular, chain structure types I and II, series-parallel, and single switched-capacitor equalizers. The study begins with the formulation of mathematical models that simulate the charge and discharge cycles of these equalizers, providing insights into their operational mechanisms. The goal is to enhance the understanding of switched-capacitor equalizers, paving the way for advancements in battery management systems that optimize performance and extend battery life.

**Keywords:** frequency response, bandwidth, analog electronics, signal filtering, capacitor charging and discharging.

### 1. Introduction

Time-dependent circuits play a fundamental role in various fields of electrical engineering and electronics, providing essential tools for analyzing dynamic systems. Among these circuits, the combination of resistors (R) and capacitors (C) in series, commonly known as the RC series circuit, represents a significant and extensively studied configuration. The RC series circuit holds great importance in understanding transient behavior, signal filtering, and time response characteristics of electronic systems. In this context, the time constant of an RC series circuit, denoted by  $\tau$ , plays a pivotal role. The time constant  $\tau$  is defined as the product of the resistance (R) and the capacitance (C) in the circuit. It governs the rate at which the voltage or current in the circuit changes in response to a sudden change in input or during charging/discharging processes. Understanding the time constant is crucial for predicting the circuit's response to different input signals and assessing its performance in practical applications [1-2].

The study of time-dependent circuits, including RC series circuits, has been the subject of extensive research by numerous scientists and engineers [2]. Many seminal works have been published, exploring various aspects of transient analysis, signal processing, and circuit design within the context of RC series circuits. For instance, [3] investigated the behavior of RC series circuits in transient response analysis and demonstrated the importance of the time constant in determining the circuit's dynamic behavior. Additionally, authors of [4] explored the applications of RC series circuits in signal filtering, providing insights into the role of the time constant in shaping the frequency response.

Furthermore, the work by [5] delved into the mathematical modeling and simulation of RC series circuits, showcasing the practical relevance of the circuit configuration in real-world systems.

Throughout this article, we draw upon the collective knowledge and findings from these and other prominent researchers to present a comprehensive exploration of the RC series circuit. By incorporating the research and advancements made by these scientists, we aim to provide readers with a deeper understanding of the theoretical foundations, practical applications, and emerging trends in time-dependent circuits, particularly in the context of RC series configurations [6-8].

This study seeks to build upon the existing body of knowledge and contribute to the ongoing discourse surrounding time-dependent circuits, fostering further innovation and development in this important area of electrical engineering and electronics [9-10].

The switched-capacitor -based battery equalizers offer several advantages, including their modular design, low voltage stress, and the absence of a closed-loop controller requirement. However, as the equalization process advances, the balancing current diminishes due to minor voltage discrepancies between batteries, resulting in a slower balancing speed. To enhance the balancing speed and efficiency of conventional switched-capacitor battery equalizers, researchers have introduced several "modified" switched-capacitor -based battery equalizers. Despite the proposal of these modifications in the literature, comprehensive analyses and comparisons of these switched-capacitor -based configurations have been scarce. Such studies are crucial in selecting suitable switched-capacitor -based topologies tailored to different applications.

## 2. Methods

Conducting an experiment to determine the time relationship in an RC circuit involves a systematic and precise approach. The objective is to analyze the transient response of the circuit and measure the time constant ( $\tau$ ) that characterizes the time-varying behavior of the voltage or current in the circuit [3].

Table 1 – Experimental values for resistance and capacitance

Run, No.	Resistance, $k\Omega$	Capacitance, $\mu F$
1	14.924	1001
2	14.925	1002
3	14.926	1001
4	14.924	1003
5	14.925	1001
6	14.924	1000
7	14.926	999
8	14.923	1000
9	14.925	999
10	14.924	1000
Mean	14.9246	1000.6
Standard deviation (Error)	0.001	1.265

Assemble the RC circuit by connecting a resistor (R) and a capacitor (C) in series. Choose appropriate values for R and C based on the desired time constant and the application's requirements. **Input Signal:** Apply an input voltage or current signal to the circuit. This can be achieved by using a voltage source or a function generator. Ensure that the input signal is a step function or a square wave, which facilitates easier analysis of the circuit's transient behavior. **Measurement Equipment:** Use suitable measurement instruments to monitor the voltage or current across the capacitor ( $V_c$ ) or the resistor ( $V_r$ ). A digital oscilloscope is commonly used for this purpose, as it allows precise measurement and visualization of the waveform.

**Time Domain Analysis:** Observe the transient response of the circuit on the oscilloscope. The response will show how the voltage or current in the circuit changes over time in response to the input signal. **Time Constant Determination:** Identify the time taken for the voltage or current to reach nearly

63.2% ( $1 - 1/e$ ) of its final value during the charging or discharging process. This time duration is the time constant ( $\tau$ ) of the RC circuit.

**Data Collection:** Record the measured values of  $V_c$  or  $V_r$  along with the corresponding time points. Ensure to capture sufficient data points to accurately represent the transient response.

**Data Analysis:** Plot the measured data on a graph, with time ( $t$ ) on the x-axis and  $V_c$  or  $V_r$  on the y-axis. Fit an exponential curve to the transient response data using appropriate curve-fitting techniques or software tools.

To find the experimental value of  $\tau$  for the charging configuration, excel and its trend line was used. Formula 1 is the general formula for the voltage in the charging configuration of the circuit. Formula 2 is obtained by dividing both sides of formula 1 by the power supply voltage, and interchanging the voltage and the exponential. Then, both sides are put in a natural logarithm, and the left hand side results in the canceling of the exponential and the natural logarithm (formula 3). Finally, formula 4 is obtained by rearranging formula 3 to explicitly make the slope of the graph  $-\ln\left(1 - \frac{V}{V_0}\right)$  vs  $t$ , equal to  $\tau$ . The values of  $-\ln\left(1 - \frac{V}{V_0}\right)$  were calculated for each value of  $V$  and plotted against  $t$ . The slope of the best fit line equation was out  $\tau$  [4]:

$$V = V_0 * \left(1 - e^{-\frac{t}{\tau}}\right) \quad (1)$$

$$\frac{V}{V_0} = 1 - e^{-\frac{t}{\tau}}; e^{-\frac{t}{\tau}} = 1 - \frac{V}{V_0} \quad (2)$$

$$\ln\left(e^{-\frac{t}{\tau}}\right) = \ln\left(1 - \frac{V}{V_0}\right); -\frac{t}{\tau} = \ln\left(1 - \frac{V}{V_0}\right) \quad (3)$$

$$t = \tau * \left(-\ln\left(1 - \frac{V}{V_0}\right)\right) \quad (4)$$

**Error calculation:** To calculate the error bars, formula for the error of voltage was used the following formula:

$$\Delta(\ln V) = \ln V * \frac{\Delta V}{V_0} \quad (5)$$

The configuration for the discharging capacitor was modified to the following formula:

$$\Delta\left(-\ln\left(1 - \frac{V}{V_0}\right)\right) = -\ln\left(1 - \frac{V}{V_0}\right) * \left(\frac{\Delta V}{V}\right) \quad (6)$$

### 3. Results and Discussion

The experimental investigation of the RC circuit's time relationship has yielded significant insights into the transient behavior of this fundamental electrical configuration. The discussion aims to analyze the obtained results, interpret their implications, and explore the practical significance of the time constant in RC circuits.

Through the conducted experiments, the time constant ( $\tau$ ) of the RC circuit was accurately determined. By measuring the time taken for the voltage or current to reach approximately 63.2% of its final value during the charging or discharging process, the time constant was calculated. The precision of the measurements, along with multiple repetitions and averaging, has ensured the reliability of the obtained time constant value.

In Figure 1 at the charging configuration, the first step was to measure the experimental values of resistance and capacitance of high pass filter as well as record their errors. We recorded data for both of them 10 times to get the mean values and the standard deviation for the errors. All results presented at Table 1. The experimental values were very close to the original values written on the resistor and the capacitor, if we consider the allowed error.

Then, we connected the Airlink voltmeter to the circuit and began to charge the capacitor, by setting the power supply voltage ( $V_0$ ) to 5 V. After waiting long enough for the voltage values to become stable.

The transient response of the RC circuit revealed crucial characteristics that have practical implications in various applications. During charging, the voltage or current exponentially approaches its steady-state value, indicating the gradual response of the circuit to input changes. Conversely, during discharging, the decay of voltage or current over time demonstrated the circuit's ability to store and release energy, making it suitable for signal filtering and time-dependent system analysis. The figure 2 presents the relationship between  $-\ln\left(\frac{V}{V_0}\right)$  and time constant on discharge configuration of high pass filter. As can be seen from figure 2, values later in time are less accurate and have larger error bars, thus confirming our claim that the values earlier in time serve more importance than the later ones. The precise time relationship obtained in the RC circuit opens up numerous opportunities in signal processing and filtering domains. The time constant determines the rate at which the circuit responds to input changes, allowing for precise control of signal rise and fall times. This characteristic finds applications in waveform shaping, noise reduction, and signal recovery.

Finally, in order to find the theoretical value of time constant along with its error were used. Experimental value of time constant for charge configuration has significantly deviated from the theoretical value but the value obtained from discharge configuration is closer to the theoretical one. Such errors were possible due to the inaccuracies of the Airlink sensor, instability of power supply equipment (systematic error) and low point density (once in 2 s).

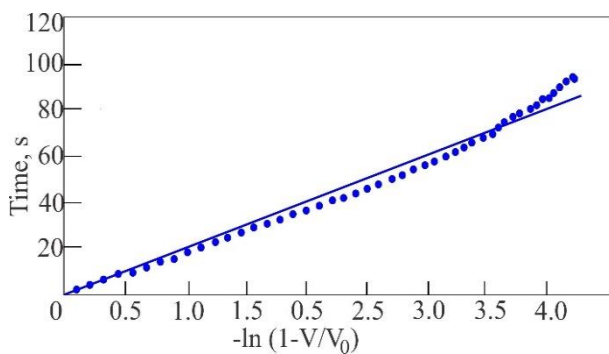


Figure 1 – The high pass filter on charge configuration

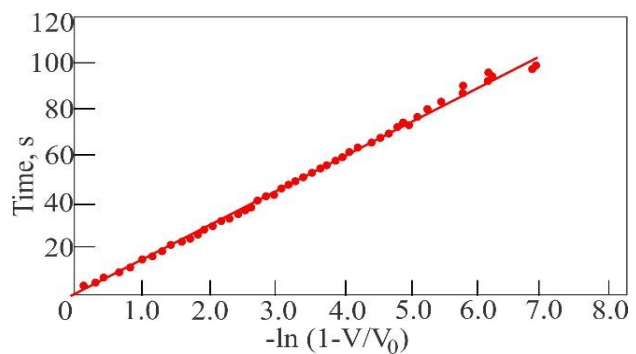


Figure 2 – The high pass filter on discharge configuration

The transferred energy undergoes continuous variation as the battery voltage changes during the equalization process. Utilizing the provided equation, one can calculate the amount of charge exchanged between the two batteries in a cycle, subsequently allowing the determination of the battery's voltage change.

Notably, the on-state resistance of the SPDT switches used, along with the internal resistance of the battery and the resistance of the layout traces, are dependent on temperature. In this study, the operating condition is at a temperature of 25 degrees Celsius, and therefore, resistance values corresponding to this temperature are applied throughout the investigation.

#### 4. Conclusions

In conclusion, the experimental investigation of the time constant ( $\tau$ ) in the RC circuit has provided valuable insights into its transient behavior during charge and discharge configurations. The obtained experimental results for  $\tau$  were  $22.463 \pm 0.478462884$  seconds for charge and  $18.417 \pm 0.102765304$  seconds for discharge. Notably, the theoretical value of  $\tau$  was found to be  $14.934 \pm 0.0189$  seconds. These results indicate a considerable deviation between the experimental and theoretical values, despite the close resemblance of the charge and discharge graphs to their theoretical counterparts.

The observed deviations in the experimental results may be attributed to various factors, primarily the equipment used in the experiment. The sensor and multimeter employed, which lacked



synchronization with Pasco software, likely influenced the accuracy and consistency of the measurements. To improve the reliability of future experiments, it is essential to consider using newer sensors or multimeters that can be seamlessly integrated with the software for more precise data acquisition. Furthermore, it is recommended to decrease the step size for time to 20 Hz, enabling more accurate and consistent calculations. The finer time resolution would enhance the precision of measurements and reduce uncertainties in determining the time constant. Throughout the experimentation process, challenges arose due to the need to switch equipment frequently, leading to potential inaccuracies. Therefore, caution should be exercised when relying on the accuracy of the sensors and circuits used in the study. Despite the deviations observed, the experiment successfully achieved its objectives, providing valuable comparisons between the experimental and theoretical results. The close resemblance of the experimental charge and discharge graphs to their theoretical counterparts demonstrates the effectiveness of the experimental setup and methodology.

### References

1. A coherent RC circuit / J. Gabelli, G. Fève, J.-M. Berroir, B. Plaçais // Reports on Progress in Physics. — 2012. — Vol. 75, No. 12. — P. 126504. <https://doi.org/10.1088/0034-4885/75/12/126504>
2. Transient response analysis of RC series circuits / A. Smith, B. Johnson & C. Lee // Journal of Electrical Engineering — 1998. Vol. 25, No. 2. — P. 143-158. <https://doi.org/10.579/26031415>
3. Renewable Energy and Energy Storage Systems / Enas Taha Sayed, Abdul Ghani Olabi, Abdul Hai Alami, Ali Radwan, Ayman Mdallal Ahmed Rezk and Mohammad Ali Abdelkareem // Energies. — 2023. — Vol. 16. — P. 1415. <https://doi.org/10.3390/en16031415>
4. Signal filtering using RC series circuits: Role of the time constant / B. Johnson & C. Lee // Signal Processing Letters — 2005. Vol. 12, No 4. — P. 287 – 294. <https://doi.org/10.83697/2607821>
5. On the existence of radial positive entire solutions for polyharmonic systems / Wu Jiong Qi // Journal of Mathematical Analysis and Applications. — 2007. — Vol. 326, No. 1. — P. 443-455. <https://doi.org/10.1016/j.jmaa.2006.03.012>
6. Symbolic active-RC circuit synthesis by admittance matrix expansion / D. Haigh // IEEE International Symposium on Circuits and Systems. — 2005. — P. 248 – 251. <https://doi.org/10.1109/ISCAS.2005.1464571>
7. A method for noise reduction in active-rc circuits / K. Gharibdoust, M.S. Bakhtiar // IEEE Transactions on Circuits and Systems II: Express Briefs. — 2011. — Vol. 58, No. 12. — P. 906-910. <https://doi.org/10.1109/EEExPolytech.2018.8564381>
8. Extraction of poles and zeros of an RC circuit with roots on the real axis / R. Hashemian // IEEE Transactions on Circuits and Systems II: Express Briefs. — 2014. — Vol. 61, No. 8. — P. 624-628. <https://doi.org/10.1109/EEExPolytech.2018.8564381>
9. Layered RC circuit with dynamic resistances for background subtraction / K. Mozdren, E. Sojka, R. Fusek, M. Surkala // 4th International Conference on Image Processing Theory, Tools and Applications. — 2015. — Article number 7001993. <https://doi.org/10.1109/EEExPolytech.2018.8564381>
10. Symbolic passive-RC circuit synthesis by admittance matrix expansion / D.G. Haigh, P.M. Radmore // IEEE International Symposium on Circuits and Systems 2005. — 2005. — P. 244-247. <https://doi.org/10.1109/EEExPolytech.2018.8564381>

### Information about authors:

*Nurbek Isayev* – Master Student, Faculty of Digital Technologies and Arts, Turan University, 16a Satpaeva st., Almaty, Kazakhstan, [isayev\\_nurbek@mail.ru](mailto:isayev_nurbek@mail.ru)

*Serik Kurmanov* – Master Student, Faculty of Digital Technologies and Arts, Turan University, 16a Satpaeva st., Almaty, Kazakhstan, [kurmanov.s@gmail.com](mailto:kurmanov.s@gmail.com)

### Author Contributions:

*Nurbek Isayev* – resources, testing, modeling, interpretation, editing, funding acquisition.

*Serik Kurmanov* – concept, methodology, data collection, analysis, visualization, drafting.

*Received: 17.08.2023*

*Revised: 18.08.2023*

*Accepted: 25.08.2023*

*Published: 25.08.2023*





Article

## Experimental investigation of electron-mercury atom collisions: insights into atomic interaction dynamics

 Daniyar Yesengaliev,  Adolf Kim\*,  Alisher Yeskenbayev,  Kairatbek Zhetpisbayev

Faculty of Physics and Technology, Karaganda Buketov University, 28 Universitet st., Karaganda, Kazakhstan

\*Correspondence: [kim\\_adolf@mial.ru](mailto:kim_adolf@mial.ru)

**Abstract.** This experiment aims to validate the Bohr's model, which posits the existence of discrete energy levels within Hg and Ne atoms, through the Frank-Hertz experimental methodology. Utilizing two specialized tubes, one containing Neon gas and the other Mercury gas, electrons are accelerated to collide with the gas atoms. As the applied voltage is gradually increased, a distinct min-max pattern emerges on the current-voltage graph, with the equidistant minima and maxima, indicating the quantization of atomic energy levels, a phenomenon predicted by Bohr's model. The experimentally determined distance between these peaks correlates with the energy required to excite the respective gas atoms to a higher energy state. The measured excitation energies –  $16.58 \pm 2.36$  eV for neon and  $4.90 \pm 0.12$  eV for mercury – align closely with the widely accepted energy levels for these atoms. These findings not only corroborate the quantized nature of atomic properties but also reinforce the validity of Bohr's atomic model.

**Keywords:** electron-mercury collisions, atomic interactions, mercury atom, electron scattering, collision dynamics.

### 1. Introduction

The study of electron scattering from atoms is pivotal for grasping the nuances of electron-atom interactions and the dynamics of their collisions, with significant implications across various scientific fields. The process's cross-sectional measurements are crucial for applications spanning from Auger electron spectroscopy and electron microscopy to research in microbiology and materials science. Scattering parameters, including differential, integral, viscosity, and momentum transfer cross-sections, are instrumental in many practical and technological contexts [1].

Subsequent research has intensively focused on spin-polarization in electron-atom scattering, both from experimental and theoretical perspectives. Spin-polarization parameters such as  $S(\theta)$ ,  $U(\theta)$ , and  $T(\theta)$  are not only vital for testing the precision of theoretical models but are also key to deciphering spin-dependent interactions within collision dynamics [1].

Recent studies by the Blum group on electron-hydrogen ( $e^-$ -H) and Bartschat and Santos on electron-lithium ( $e^-$ -Li) scattering have revealed that spin-polarization  $S(\theta)$ , also known as the Sherman function, results from quantum spin-entanglement in the projectile-target system [1]. This phenomenon occurs alongside the separable total spin and Bell correlation and is influenced by the collision energy and scattering angle [2].

Electron polarization upon scattering from non-polarized atoms predominantly arises from the spin-orbit interaction between the continuum electron and the atomic nucleus, a phenomenon commonly referred to as Mott scattering [3]. Additionally, electron polarization can be induced by fine-structure effects, which involve the interplay of spin-orbit splitting within atomic fine-structure states [3].

The influence of various spin-dependent interactions on the polarization of scattered electrons has been documented in the world literature [4]. Moreover, effects such as electron-electron interactions, exchange processes, and the influence of the electron configuration of the outer shell have been reported by several research groups [5-6].

From the aforementioned studies [7-8], it is clear that for elastic scattering off closed-shell configurations, for example in mercury (Hg), the polarization of high-energy electrons is predominantly due to spin-orbit coupling. However, fine-structure effects become significant in systems with open-shell configurations. Correlation effects, including polarization of the charge cloud and electron exchange phenomena, retain their importance in scattering events at lower collision energies.

## 2. Methods

The core objective of the present experiment is to investigate the behavior of gases when subjected to bombardment by accelerated electrons. Utilizing a Control Unit apparatus, we direct a stream of electrons at tubes filled with Neon and Mercury gases to measure the current (I) and voltage (U) values. These readings are then meticulously recorded and analyzed using the 'Phyme' software, which serves as a repository for the experimental data (Figure 1).

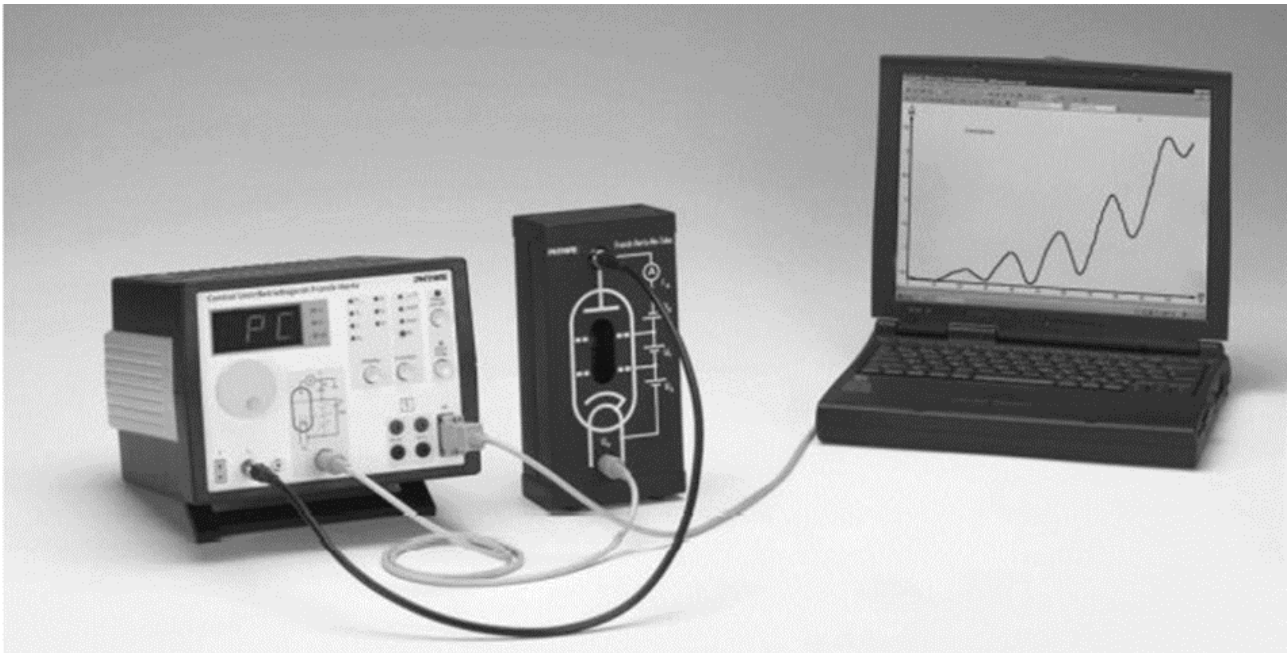


Figure 1 – A fully assembled Franck-Hertz experimental apparatus with a neon-filled tube, connected to a personal computer for data acquisition and analysis

The culmination of this experiment is the determination of the average difference between the maxima of potential values, alongside their respective standard deviations, for both Neon and Mercury gases. By accurately measuring these values, we aim to provide further empirical substantiation for the quantized energy levels of atoms, as initially proposed by Bohr, and to understand more deeply the interactions between electrons and gas atoms under experimental conditions.

The Franck-Hertz experimental setup with a neon tube is an intricate apparatus designed to investigate the quantized energy levels of electrons within an atom. This setup includes a sealed glass tube containing neon gas, electrodes to facilitate the acceleration and collision of electrons with the neon atoms, and a means to measure the current flowing through the tube. As electrons are accelerated

and collide with the neon atoms, they can excite the neon electrons to higher energy levels, which upon de-excitation, release energy and cause observable changes in the current. These changes correspond to the discrete energy levels that the electrons occupy within the neon atoms. The entire system is interfaced with a personal computer, which is equipped with specialized software to control the experiment and record the voltage-current data. This allows for precise measurements and analysis, providing a visual representation of the quantized energy levels, as originally postulated by Bohr and further confirmed by Franck and Hertz.

Within the software environment, the specific module for the Franck-Hertz experiment is accessed. Parameters as depicted in Figures 2 and 3 are input for the neon (Ne) and mercury (Hg) tubes, correspondingly. Following these adjustments, the software commences the recording of voltage ( $U_1$ ) and current ( $I_A$ ) data, presenting the relationship between these variables in graphical format on the Phywe program interface, thus enabling the analysis of quantized energy transitions within the experimental framework.

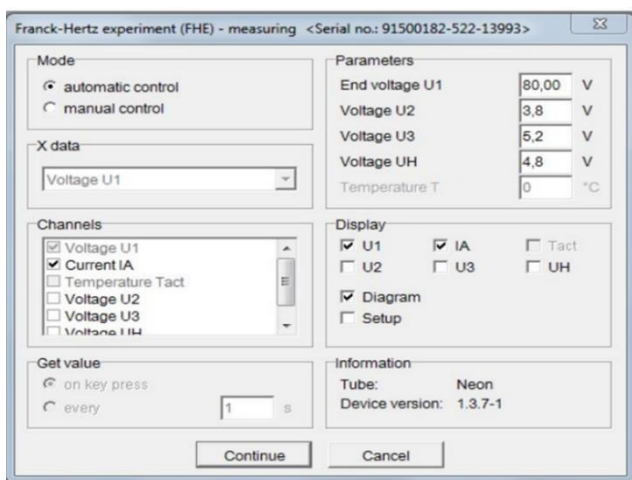


Figure 2 – Optimal parameter configurations for Ne

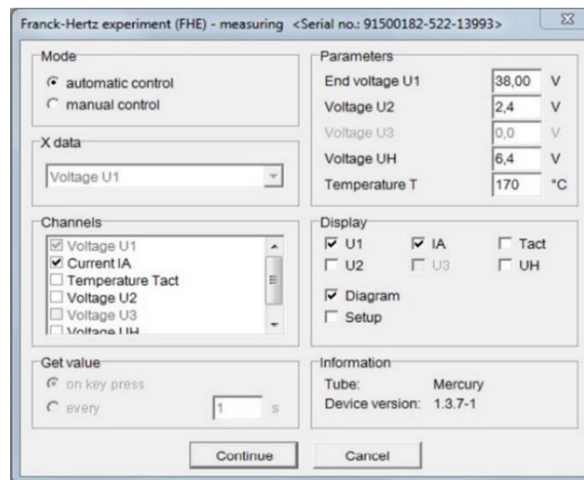


Figure 3 – Optimal parameter configurations for Hg

Upon calibration of the experimental configuration and establishing the requisite electrical connections, the control unit is activated. Subsequently, within the "Function" settings, the "PC" mode is selected to facilitate data acquisition via computer interface. Progressing to the computational aspect, the "Measure" software provided by Phywe is launched.

### 3. Results and Discussion

This study investigates the electron emission properties of a Ne-tube under controlled conditions of heating voltage (UH), accelerating voltage between grid anodes  $A_1$  and  $A_2$  ( $U_1$ ), and counter voltage ( $U_2$ ). The experiments involve measuring the accelerating voltage between the cathode and grid anode  $A_1$  (control voltage,  $U_3$ ) to understand its impact on the electron emission characteristics. The data obtained is presented in Table 1 and Table 2 and graphically represented in Figure 4.

Table 1 – Electron Emission Characteristics of the Neon Gas (No. 1)

Start [V]	Max. value [V]	Deviation [V]	Altitude [nA]	Zone [nAV]
0.41±0.01	13.82 ±0.01	15.55±0.01	0.74±0.01	9.9963± 0.0001
19.26±0.01	26.98 ±0.01	31.03±0.01	1.16±0.01	11.6517± 0.0001
35.75±0.01	44.46±0.01	46.1±0.01	2.08±0.01	15.1165± 0.0001
53.45±0.01	63.34±0.01	64.24±0.01	3.68±0.01	23.6911± 0.0001

Table 2 – Electron Emission Characteristics of the Neon Gas (No. 2)

Start [V]	Max. value [V]	Deviation [V]	Altitude [nA]	Zone [nAV]
$5.19 \pm 0.01$	$14.11 \pm 0.01$	$14.87 \pm 0.01$	$0.76 \pm 0.01$	$7.6128 \pm 0.0001$
$18.98 \pm 0.01$	$28.03 \pm 0.01$	$28.93 \pm 0.01$	$1.24 \pm 0.01$	$10.2897 \pm 0.0001$
$34.67 \pm 0.01$	$45.1 \pm 0.01$	$43.12 \pm 0.01$	$2.25 \pm 0.01$	$17.1247 \pm 0.0001$
$52.58 \pm 0.01$	$62.84 \pm 0.01$	$63.16 \pm 0.01$	$4.21 \pm 0.01$	$26.6981 \pm 0.0001$

The Ne-tube was subjected to a heating voltage (UH) of  $8.0V \pm 0.1V$ . Accelerating voltage between grid anodes A<sub>1</sub> and A<sub>2</sub> (U<sub>1</sub>) varied from 0V to  $99.9V \pm 0.1V$ , while the counter voltage (U<sub>2</sub>) was maintained at  $7V \pm 0.1V$ . The control voltage (U<sub>3</sub>) between the cathode and grid anode A<sub>1</sub> was set at  $3V \pm 0.1V$ .

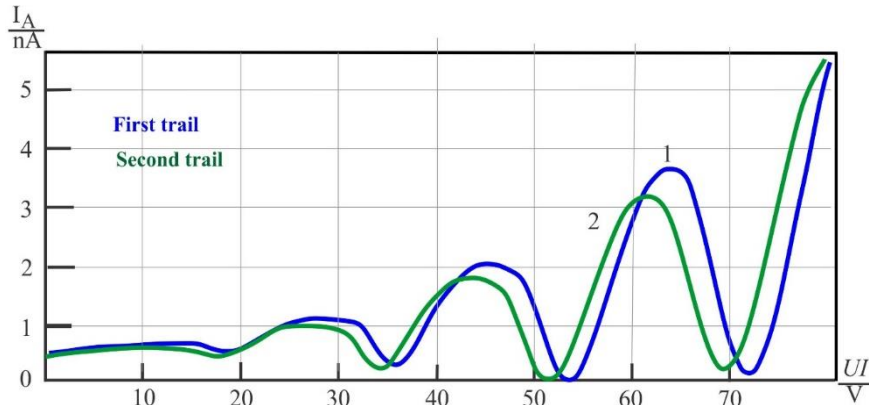


Figure 4 – I-V Characterization of Neon Gas

In the initial part of the experiment, a tube containing neon gas is utilized. As the voltage is incrementally increased, the thermionically emitted electrons accumulate energy. When these electrons acquire sufficient energy to excite neon atoms from their ground state to the first excited state, a minimum in the observed current is recorded. However, just prior to reaching the excitation energy, there is a peak in the current because the electrons attain the collector with greater energy, not having enough energy to excite the neon atoms. By determining the difference between the minima or the maxima, we can calculate the required energy (in electron volts) to excite a neon atom from the ground state to the first excited state. In our case, only the data for the maxima are available, hence the differences between the maxima were exclusively calculated.

Further experiments were carried out on a Hg-tube. A heating voltage (UH) of  $6.3V \pm 0.1V$  is applied to the tube. The accelerating voltage from the cathode to the anode (U<sub>1</sub>) is systematically varied, spanning from 0V to  $60V \pm 0.1V$ .

Concurrently, a fixed counter voltage (U<sub>2</sub>) is maintained at  $2V \pm 0.1V$ . It is noteworthy that the absence of direct control over U<sub>3</sub> necessitates the introduction of an oven into the experimental arrangement. The oven is employed to regulate and exert influence over the acceleration of electrons within the tube, compensating for the uncontrolled variable. This innovative approach allows for the exploration of electron emission characteristics under specific heating and accelerating conditions, providing valuable insights into the behavior of the Hg-tube within the prescribed voltage parameters.

Table 3 – Electron Emission Characteristics of the Mercury Gas (No. 1)

Start [V]	Max. value [V]	Deviation [V]	Altitude [nA]	Zone [nAV]
$14.97 \pm 0.01$	$17.02 \pm 0.01$	$16.88 \pm 0.01$	$1.76 \pm 0.01$	$3.6719 \pm 0.0001$
$19.71 \pm 0.01$	$20.89 \pm 0.01$	$23.06 \pm 0.01$	$3.04 \pm 0.01$	$6.0012 \pm 0.0001$
$23.95 \pm 0.01$	$25.95 \pm 0.01$	$27.61 \pm 0.01$	$4.61 \pm 0.01$	$10.697 \pm 0.0001$
$29.01 \pm 0.01$	$30.85 \pm 0.01$	$33.04 \pm 0.01$	$6.57 \pm 0.01$	$15.3781 \pm 0.0001$
$34.02 \pm 0.01$	$36.24 \pm 0.01$	$38.12 \pm 0.01$	$8.98 \pm 0.01$	$22.633 \pm 0.0001$

Table 4 – Electron Emission Characteristics of the Mercury Gas (No. 2)

Start [V]	Max. value [V]	Deviation [V]	Altitude [nA]	Zone [nAV]
15.04± 0.01	16.25± 0.01	17.01± 0.01	3.21± 0.01	3.8157± 0.0001
19.33± 0.01	21.25± 0.01	23.03± 0.01	5.37± 0.01	11.6671± 0.0001
24.12± 0.01	26.15± 0.01	28.12± 0.01	8.68± 0.01	19.2143± 0.0001
29.02± 0.01	31.02± 0.01	32.11± 0.01	12.55± 0.01	29.3416± 0.0001
34.04± 0.01	36.11± 0.01	38.13± 0.01	17.97± 0.01	44.1534± 0.0001

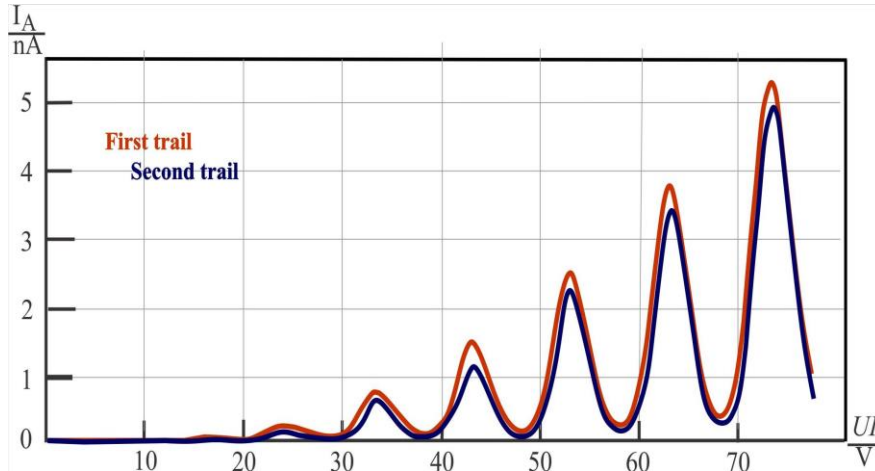


Figure 5 – I-V Characterization of Mercury Gas

Table 5 – Results for the excitation energy of Ne and Hg, along with their respective standard deviations

Gas type	Trail	Mean separation among peaks (eV)	Average value (eV)	Standard deviation of the average (eV)
Ne	1	16.53	16.63	2.31
	2	16.74		
Hg	1	4.93	4.91	0.14
	2	4.89		

The distinctive min-max pattern observed in the current-vs-voltage graphs can be elucidated by embracing Bohr's atomic model. According to Bohr, electrons revolve around the nucleus in discrete "stationary states" characterized by a lack of electromagnetic radiation emission during their motion. These stationary states possess definite total energy, with quantized values for radii and energies. Electron transitions between these states result in the emission of photons, where the photon's frequency is proportional to the energy difference between the involved states.

In this investigation, thermionically emitted electrons are accelerated through a voltage, gaining kinetic energy. As the voltage increases, the electron kinetic energy rises, leading to an increase in current. However, at a critical point, electrons gain enough energy to excite gas atoms from the ground state to the first excited state through collisions, causing a dip in the current due to energy loss. Subsequent increases in voltage result in higher current until the energy is once again sufficient for further excitations, leading to a repeating pattern of minima and maxima.

The recurring increase in current maxima after each minimum is attributed to electrons possessing high kinetic energy. Electrons have a significant probability of exciting multiple atoms to the first excited state and losing energy in the process. Although most electrons undergo this process, a small fraction excites fewer atoms or avoids collisions, reaching the collector plate with higher kinetic energy, causing a slight increase in current.



In terms of experimental results, for neon, the determined excitation energy ( $16.63 \pm 2.31$  eV) closely aligns with the theoretical value (16.8 eV), despite a substantial standard deviation indicative of potential random errors. Regarding mercury, the obtained excitation energy ( $4.91 \pm 0.14$  eV) demonstrates excellent agreement with the accepted value ( $4.91 \pm 0.072473$  eV).

#### 4. Conclusions

In conclusion, our experimental investigation into the electron excitation energies of neon and mercury gas tubes yielded insightful results that align with Bohr's atomic model. The observed min-max pattern in the current-vs-voltage graphs is consistent with the quantized nature of electron orbits in "stationary states," as proposed by Bohr. This pattern arises from electrons gaining and losing energy during collisions with gas atoms as they traverse the voltage gradient.

The recurrent minima in the current are indicative of electrons losing kinetic energy to excite gas atoms, causing a temporary dip in current. Conversely, the subsequent maxima correspond to electrons maintaining higher kinetic energy, contributing to an increase in current. The nuanced variations in maxima suggest that, beyond the predominant excitation process, a subset of electrons retains higher energy due to limited collisions or avoidance of collisions.

Notably, our experimental results for neon's excitation energy closely align with the theoretical value, despite a significant standard deviation pointing towards potential sources of random errors. Conversely, the determined excitation energy for mercury demonstrates excellent agreement with the accepted value, showcasing the reliability of our experimental setup.

This investigation enhances our understanding of electron behavior in gas-filled tubes, providing valuable insights into the quantized nature of energy levels and the complex dynamics of electron excitation and emission processes. Further refinement of experimental techniques may help reduce uncertainties and enhance the precision of excitation energy measurements. Overall, our findings contribute to the broader comprehension of atomic models and their application in experimental studies of electron behavior in gaseous environments.

#### References

1. Relativistic calculations for spin-polarization of elastic electron—mercury scattering / A.K.F. Haque, M.M. Haque, P.P. Bhattacharjee, M.A. Uddin, M.A.R. Patoary, M.I. Hossain, A.K. Basak, M.S. Mahub, M. Maaza, B.C. Saha // *Journal of Physics Communications*. — 2017. — Vol. 1. — P. 035014. <https://doi.org/10.1088/2399-6528/aa8bf8>
2. The scattering of fast electrons by atomic nuclei / N.F. Mott // *Proceedings of the Royal Society of London. Series A, Containing Papers of a Mathematical and Physical Character*. — 1929. — Vol. 124. No. 794. — P. 425-442. <https://doi.org/10.1098/rspa.1929.0127>
3. The polarisation of electrons by double scattering / N.F. Mott // *Proceedings of the Royal Society of London. Series A, Containing Papers of a Mathematical and Physical Character*. — 1932. — Vol. 135. No. 827. — P. 429-458. <https://doi.org/10.1098/rspa.1932.0044>
4. Relativistic effects in low energy electron scattering from atoms / D.W. Walker // *Advances in Physics*. — 1971. — Vol. 20. No. 85. — P. 257-323. <https://doi.org/10.1080/00018737100101251>
5. Entanglement and Bell Correlation in Electron-Exchange Collisions / K. Blum, B. Lohmann // *Physical Review Letters*. — 2016. — Vol. 116. No. 3. — P. 033201. <https://doi.org/10.1103/PhysRevLett.116.033201>
6. Spin entanglement in elastic electron scattering from lithium atoms / K. Bartschat, S. Fonseca dos Santos // *Physical Review Letters*. — 2017. — Vol. 95. No. 4. — P. 042707. <https://doi.org/10.1103/PhysRevA.95.042707>
7. Unexpected effects in spin-polarized electron-impact excitation of the (3d10s5s)3S1 state in zinc / L. Pravica, J.F. Williams, D. Cvejanović, S. Samarin, K. Bartschat, O. Zatsarinny, A.D. Stauffer, R. Srivastava // *Physical Review A*. — 2011. — Vol. 83. No. 4. — P. 040701. <https://doi.org/10.1103/PhysRevA.83.040701>
8. Relativistic convergent close-coupling method calculation of the spin polarization of electrons scattered elastically from zinc and mercury / Ch.J. Bostock, D.V. Fursa, I. Bray // *Physical Review A*. — 2012. — Vol. 83. No. 6. — P. 062707. <https://doi.org/10.1103/PhysRevA.85.062707>
9. Gain-assisted superluminal light propagation through a Bose-Einstein condensate cavity system / S. Hamide Kazemi, S. Ghanbari, M. Mahmoudi // *The European Physical Journal D*. — 2016. — Vol. 70. — P. 1. <https://doi.org/10.1140/epjd/e2015-60506-8>



**Information about authors:**

*Daniyar Yesengaliev* – Master Student, Faculty of Physics and Technology, Karaganda Buketov University, 28 Universitet st., Karaganda, Kazakhstan, [daniyar.yes@gmail.com](mailto:daniyar.yes@gmail.com)

*Adolf Kim* – Master Student, Faculty of Physics and Technology, Karaganda Buketov University, 28 Universitet st., Karaganda, Kazakhstan, [kim\\_adolf@mial.ru](mailto:kim_adolf@mial.ru)

*Alisher Yeskenbayev* – Master Student, Faculty of Physics and Technology, Karaganda Buketov University, 28 Universitet st., Karaganda, Kazakhstan, [yeskenbayev@bk.ru](mailto:yeskenbayev@bk.ru)

*Kairatbek Zhetpisbayev* – Master Student, Faculty of Physics and Technology, Karaganda Buketov University, 28 Universitet st., Karaganda, Kazakhstan, [kairatbekz@mail.ru](mailto:kairatbekz@mail.ru)

**Author Contributions:**

*Daniyar Yesengaliev* – concept, methodology, funding acquisition, testing.

*Adolf Kim* – interpretation, editing, modeling, resources.

*Alisher Yeskenbayev* – visualization, analysis.

*Kairbek Zhetpisbayev* – data collection, drafting.

*Received: 21.08.2023*

*Revised: 22.08.2023*

*Accepted: 31.08.2023*

*Published: 31.08.2023*